Pis'ma v ZhETF, vol.65, iss.9, pp.722 - 727

SHOCK WAVE STRUCTURE IN SIMPLE LIQUIDS

S.I.Anisimov[1)], *V.V.Zhakhovskii*[2)], *V.E.Fortov*

Landau Institute for Theoretical Physics, RAS

117334 Moscow, Russia

Submitted 10 April, 1997

Shock wave structure in a liquid is studied using molecular dynamics simulation method. The interaction between atoms is described by the Lennar-Jones (6-12) potential. In contrast to earlier works, the simulation is performed in the frame connected with shock wave front. This approach reduces non-physical fluctuations and makes it possible to calculate the distribution functions of kinetic and potential energy for several cross sections within the shock layer. The profiles of flow variables and their fluctuations are found. The surface tension connected with pressure anisotropy within the shock front is calculated. It is shown that the main contribution to the surface tension coefficient comes from the mean virial.

PACS: 02.70.Ns, 62.50.+p

The internal structure of shock waves has been extensively investigated both, experimentally and theoretically (see, e.g., [1-13]). Earlier theoretical studies of shock wave structure were based either on hydrodynamic approximation (which is valid for weak shock waves only) [2-5], or on the Boltzmann kinetic equation (which holds for rarefied gases only) [6-8]. Thus, only certain limiting cases have been studied. More recently, the direct Monte-Carlo and molecular dynamics (MD) simulation methods have been employed to study the shock wave structure in solids, liquids, and dense gases (see [9-13]). These simulation works have, however, the common disadvantage of large nonphysical fluctuations. Owing to these fluctuations, important characteristics of the shock layer (e.g., the evolution of velocity distribution function across the layer) have not been studied up to now. There are two main reasons for high level of fluctuations in the MD shock wave simulations. First, in the major part of simulation works, a standard statement of the problem is used, when a shock wave is generated in a fluid at rest by a moving piston. As the result, the shock wave is non-stationary in the laboratory frame. Second, the number of particles in the MD cell is typically about few thousands which is not sufficient for quantitative description of shock wave structure. In the present work we use a special potential configuration, which makes it possible to generate a shock wave at rest in the laboratory frame, and employ the so-called Langevin thermostat to create the upstream fluid flow with given mass velocity and temperature. The number of atoms in our simulations was typically an order of magnitude larger than in the works [10,11,13]. This approach substantially improves the quality of simulation and allows to trace the evolution of the kinetic and potential energy distributions across the shock layer. Since the kinetic energy distribution within the shock layer is nonequilibrium, the concept of local temperature is not applicable. We use in this work the mean square fluctuations of the longitudinal and transverse velocity components to describe the transformation of kinetic energy of the upstream flow into thermal energy of the

[1)]e-mail: anisimov@itp.ac.ru

[2)]e-mail: basil@landau.ac.ru

downstream flow. We employ also the pair correlation function (which depends on the transverse coordinates (x, y)), calculated for several planes z =const within the shock layer, to describe the evolution of the fluid structure during the shock compression.

The interaction of atoms in a simple liquid is described in this work by the Lennard-Jones (6-12) potential (LJ-potential):

$$U(r) = 4\varepsilon[(\sigma/r)^{12} - (\sigma/r)^{6}]. \tag{1}$$

We will use thereafter the MD units determined through the parameters of the potential (1). The results of calculations will then be valid for any LJ-fluid. The parameter σ is chosen as the unit of length, and the parameter ε as the unit of energy. It is convenient to chose the particle mass equal to 48 MD units. The units of time and velocity are then $\sigma\sqrt{m/48\varepsilon}$ and $\sqrt{48\varepsilon/m}$, respectively. For example, for argon atoms, the unit of length is $\sigma = 0.3405$ nm, the unit of time is 0.31144 ps, the unit of energy (temperature) is $\varepsilon = 1.654 \cdot 10^{-14}$ erg = 119.8 K, the unit of velocity is 1.0933 km/s, and the unit of density is 1.6825g/cm^3. The rectangular MD simulation cell is similar to that used in our previous work [14]. It has the dimensions $L_x \times L_y \times 2L_z$ with periodic boundary conditions imposed along all the three coordinate axes. The flow velocity is directed along the z-axis. Short-range potentials U^+ and U^- are located at the opposite sides of the MD cell and satisfy the condition that the forces $\partial U^+/\partial z = \partial U^-/\partial z = 0$ at $z = \pm L_z$. Since the accelerating U^+ and decelerating U^- potentials have different magnitudes, the atoms crossing the boundary of MD cell change their energy. To form a uniform upstream flow with given temperature T_1 and mass velocity $V_1 = V_{1z}$, the Langevin thermostat [15] is used. The thermostat constitutes a part of MD cell, in which the atoms are subjected to Langevin force

$$dv_i^a/dt = \beta(V_1\delta_{iz} - v_i^a) + \xi_i(t) \tag{2}$$

where β is the friction coefficient, $\xi_i(t)$ is Gaussian random force ("white noise"), the subscript $i = x, y, z$, and the superscript a numbers the atoms. To obtain a prescribed temperature T_1, the parameters of Eq.(2) should satisfy the condition $\langle \xi_i^2 \rangle = 2\beta T_1/\Delta t$, where Δt is the time step of integration, and the temperature is expressed in energy units. The equations of motion are integrated using the 8th order Stoermer method, which was previously used in Refs.[14, 16, 17] for MD simulation of shock waves in L-J-gases and the liquid-gas phase transition. The details of the algorithm are described in [14].

Consider typical examples of simulation. The parameters of shock waves for two different Mach numbers ($M \approx |V_1|$ for liquid argon) are presented in Table.

$\lvert V_1\rvert$	$\lvert V_2\rvert$	n_1	n_2	T_1	T_2	l_s	γ_T	γ_u	γ
2.48	1.61	0.76	1.17	1.03	7.86	1.95	5.90	40.93	46.83
4.95	2.74	0.76	1.37	1.04	48.65	1.42	49.36	120.14	169.50

The shock wave thickness presented in Table is defined as

$$l_s = (n_2 - n_1)/(dn/dz)_{max}.$$

In Fig.1, the profiles of mean square fluctuations of the longitudinal (curve n) and transverse (curve τ) components of molecular velocity are presented. The

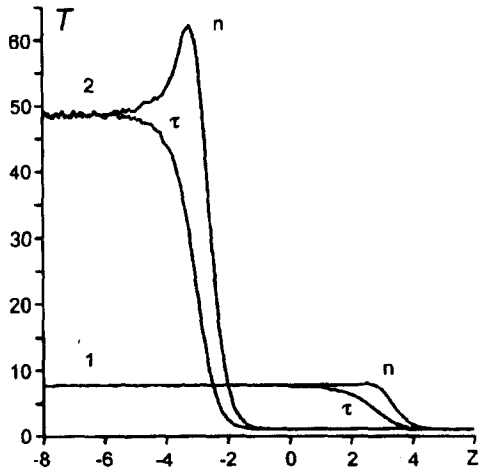

Fig.1. Spatial profiles of mean-square fluctuations of the longitudinal (n) and transverse (τ) velocity components in stationary shock waves. Upstream velocities are curve *1* – $|V_1| = 2.48$ and *2* – $|V_1| = 4.95$

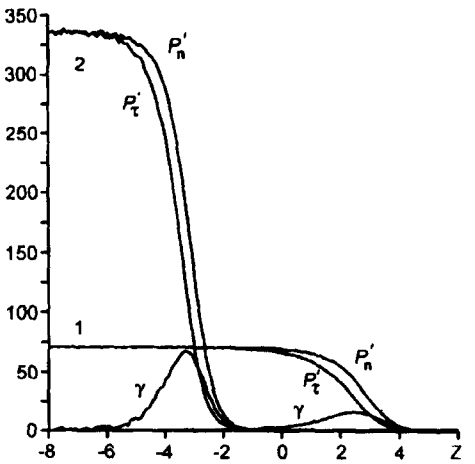

Fig.2. Spatial profiles of normal (n) and tangential (τ) pressure components in stationary shock waves

simulation reveals that the fluctuation of the longitudinal velocity component, $T_n = 48\left\langle (v_z - \overline{v_z})^2 \right\rangle$, grows faster than the fluctuation of the transverse component, $T_\tau = 48\left\langle v_x^2 \right\rangle$. Similar phenomenon has been observed in dense gases [16]. It can be attributed to the fact that the transformation of the energy of ordered motion along the z-axis into the energy of random (thermal) motion along the x, y-axes requires large-angle scattering. This transformation proceeds slowly since it is connected with high energy tail of particle distribution. By contrast, a similar process resulting in the thermalization of the z-component of velocity is not much connected with the tail of the distribution function, and has a higher rate. Note that the function $T_n(z)$ has a maximum within the shock front at sufficiently high Mach number. The difference between T_n and T_τ leads to the anisotropy of pressure within the shock layer and to the effect similar to the surface tension. The pressure in the case under consideration is a symmetric tensor, rather than a scalar. In general nonequilibrium case, the pressure tensor can be calculated using the procedure described in Refs.[18, 19] and the results of MD simulation. The components of pressure are given by

$$P_n(z) = n(z)T_n(z) - \frac{1}{2S}\left\langle \sum_{a \neq b} \frac{z_{ab}^2}{r_{ab}} \frac{\partial U(r_{ab})}{\partial r_{ab}} \delta(z - z_a) \right\rangle, \tag{3a}$$

$$P_\tau(z) = n(z)T_\tau(z) - \frac{1}{2S}\left\langle \sum_{a \neq b} \frac{(x_{ab}^2 + y_{ab}^2)}{2r_{ab}} \frac{\partial U(r_{ab})}{\partial r_{ab}} \delta(z - z_a) \right\rangle, \tag{3b}$$

where S is the area of MD cell in x, y-plane. The coefficient of surface tension is defined as

$$\gamma = \int_{-\infty}^{\infty} (P_n - P_\tau) dz. \tag{4}$$

The virial terms of normal and tangential components of pressure P_n, P_τ and the difference between them $\gamma(z)$ are calculated in the same way as in Ref.[16] and presented in Fig.2. Notice that in the case of liquids the main contribution to γ originates from potential energy of particle interaction (second terms in Eqs.(3a) and (3b)), whereas in gases it was connected with kinetic energy of particles (first terms in Eqs.(3a) and (3b)) [16,20]. The values of "potential" (γ_u) and "kinetic" (γ_T) contributions to the surface tension γ are given in Table. As is clear from Eq.(4), the surface tension is a small effect, proportional to shock wave thickness. Corresponding correction to the downstream pressure P_2 is of the order of $P_2 l_s/R$, where R is the radius of curvature of the shock wave. An excess pressure behind the front of spherical shock wave observed in [21] may be attributed to the surface tension (see Ref. [20]).

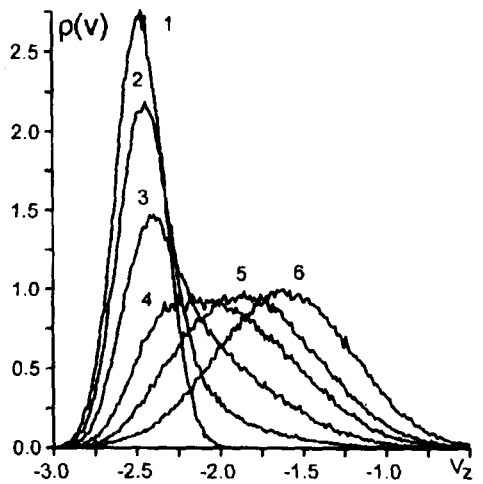

Fig.3. Distribution functions of the z-component of velocity in different layers normal to the z-axis: *1)* $-12 < z < -11.8$, *2)* $2 < z < 2.2$, *3)* $2.5 < z < 2.7$, *4)* $3 < z < 3.2$, *5)* $3.5 < z < 3.7$, *6)* $12 < z < 12.2$. Upstream velocity $|V_1| = 2.48$

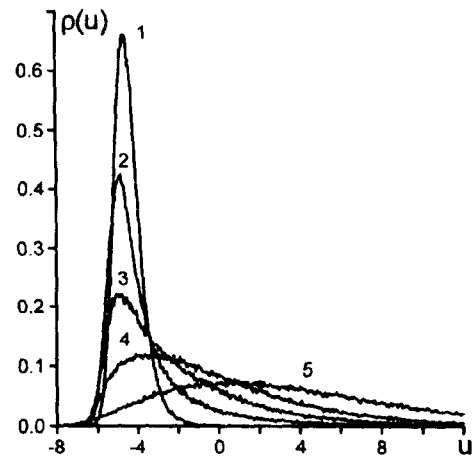

Fig.4. Distribution functions of the potential energy in different layers normal to the z-axis: *1)* $-12 < z < -11.8$, *2)* $2.5 < z < 2.7$, *3)* $3 < z < 3.2$, *4)* $3.5 < z < 3.7$,*5)* $12 < z < 12.2$. Upstream velocity $|V_1| = 2.48$

The effect of surface tension may play an important role in the problem of shock wave stability. For a plane shock wave, considered as a gas dynamics discontinuity, the problem of stability with respect to the corrugation perturbations was first considered in [22]. The analysis showed that, depending on slope of the Hugoniot curve, the wave may be stable, unstable, or neutrally stable. In the latter case, small effects connected with finite shock wave thickness might affect the result. In studies of shock wave stability, it is natural to consider the gas dynamic discontinuity as a limiting case of the shock wave possessing the internal structure. In particular, the stability of weak shock wave can be studied using the Navier–Stokes equations. The effects of the order of l_s/λ, where λ is the perturbation wavelength, would be automatically taken into account in this study. This approach, however, can not be directly applied to a shock wave of arbitrary amplitude in the medium with arbitrary equation of state (which is of prime interest for shock instability studies). An alternative approach, which can be used

in this case, is to study the stability problem for a gas dynamic discontinuity and incorporate the effect of finite shock thickness into the boundary conditions in the form of surface tension on curved shock surface. The latter approach was used in Refs. [20, 23] to account for experimentally observed instability of the relaxation zone in ionising shock waves in gases (note that in this case the relevant stability analysis can be performed in hydrodynamic approximation). It is clear, that the method based on the concept of surface tension offers considerable scope for the study of neutrally stable (according to [22]) shock waves in liquids and solids. The above calculated values of γ can be used in this study.

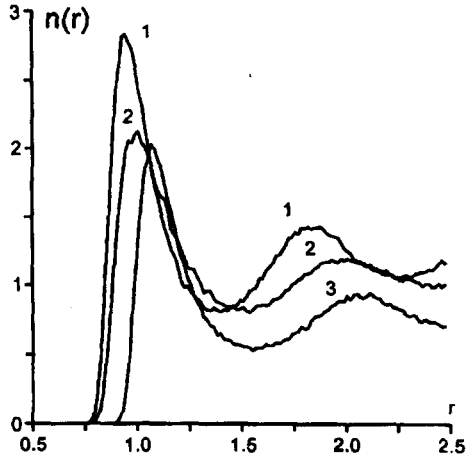

Fig.5. The pair correlation function in the upstream *1*) $-12 < z < -11.8$ and downstream *3*) $12 < z < 12.2$ flows, and in the center of shock layer *2*) $2 < z < 2.2$, $|V_1| = 2.48$

The evolution of particle distribution over the velocity component v_z across the shock layer for $M \approx 2.5$ is shown in Fig.3. It is easily seen that the distribution functions in different planes normal to the z-axis are deviated widely from corresponding bimodal distribution. A detailed comparison of the distribution functions derived from MD simulation with those calculated using the bimodal distribution shows that, contrary to the case of gases [16], the deviation slightly decreases with the Mach number increasing.

In Fig.4 the probability density for the potential energy in several planes z =const within the shock layer is shown. It is seen that the mean value of potential energy is negative in the upstream flow and positive in the downstream flow, i.e., the shock compression of a liquid results in the change of sign of interparticle forces. Corresponding change in the structure of liquid is demonstrated in Fig.5, where the evolution of the pair correlation function is shown. We consider the correlation function that depends on two-dimensional distance r between atoms in a plane z =const. It is seen that the structure of the correlation functions is totally different from that observed in [16] for the shock wave in a dense gas. The curves *1* and *2* are closely similar to each other, and typical for liquid state. The curve *3* shows that a short-range order exists in the shock-compressed fluid. Since the potential energy in the downstream flow is positive, the shock-compressed fluid resembles a system of closely packed spheres.

The authors would like to express their gratitude to A.F.Andreev, I.M.Khalatnikov and L.P.Pitaevskii for valuable discussions. The work was support-

ed by the Cariplo Foundation for Scientific Research and Russian Basic Research Foundation.

---

1. E.Muntz and L.M.Harnett, Phys.Fluids **12**, 2027 (1969).
2. L.D.Landau and E.M.Lifshitz, *Fluid Mechanics*, Pergamon Press, Oxford, 1959.
3. H.W.Liepman, R.Narashima, and M.T.Chahine, Phys.Fluids **5**, 1313 (1962).
4. D.Gilbarg and D.Paolucci, J. Ratl. Mech. Anal. **2**, 617 (1953).
5. C.Muckenfuss, Phys. Fluids **5**, 1325 (1962).
6. I.E.Tamm, Trudy FIAN **29**, 317 (1965).
7. H.M.Mott-Smith, Phys. Rev. **82**, 885 (1951).
8. W.Fiszdon, R.Herczynski, and Z.Walenta, in: *Rarefied Gas Dynamics*, Eds. M.Becker and M.Fiebig, Porz-Wahn, DFVLR Press, 1974, p.B23.
9. G.A.Bird, Phys.Fluids **13**, 1172 (1979).
10. W.G.Hoover, Phys. Rev. Lett. **42**, 1531 (1979).
11. B.L.Holian, W.G.Hoover, B.Moran, and G.K.Straub, Phys. Rev. **A22**, 2798 (1980).
12. E.Salomons and M.Marechal, Phys. Rev. Lett. **69**, 269 (1992).
13. M.Koshi, T.Saito, H.Nagoya, K.Gakkaishi, **55**, 229 (1994).
14. V.V.Zhakhovskii and S.I.Anisimov, JETP **84**, N4, (1997).
15. D.W.Heerman, *Computer Simulation Methods in Theoretical Physics*, Springer Verlag, Berlin - New York, 1986.
16. V.V.Zhakhovskii, K.Nishihara, and S.I.Anisimov, Phys. Rev. Lett., in press.
17. S.I.Anisimov, V.V.Zhakhovskii, JETP Lett. **57**, 99 (1993).
18. J.S.Rowlinson and B.Widom, *Molecular Theory of Capillarity*, Clarendon Press, Oxford, 1982.
19. P.Resibois and M.De Lechner, *Classical Kinetic Theory of Fluids*, J.Wiley and Sons, New York, 1977.
20. A.G.Bashkirov, *Nonequilibrium Statistical Mechanics of Heterogeneous Fluid Systems*, CRC Press, Boca Raton - London - Tokyo, 1995.
21. W.M.Kornegay, J.D.Fridman, and W.C.Worthington, in: *Proc. 6th Intern. Symp. Rarefied Gas Dynamics*, **1**, 863 (1969).
22. S.P.Dyakov, Zhur. Exp. Theor. Phys. **27**, 288 (1954).
23. A.G.Bashkirov, Phys. Fluids **A3**, 960 (1991).